A note on predator prey dynamics in radiocarbon datasets

Nimrod Marom*[1], Uri Wolkowski[1]

[1] Laboratory of Archaeozoology, University of Haifa, Haifa, Israel.

*Corresponding author
Correspondence: nmarom2@univ.haifa.ac.il

ABSTRACT

Predator-prey interactions have been a central theme in population ecology for the past century, but real-world data sets only exist for recent, relatively short (<100 years) time spans. This limits our ability to study centennial/millennial-scale predator-prey dynamics. We propose that regional radiocarbon databases can be used to reconstruct a signal of predator-prey population dynamics in deep time, overcoming this limitation. We support our argument with examples from Pleistocene Beringia and the Holocene Judean Desert.

Keywords: radiocarbon, paleozoology, Judean Desert, Beringia.

Introduction

Predator-prey interactions are a fundamental topic in theoretical ecology (May, 2001 [1974]), nature conservation (Johnson et al., 2019; Southall et al., 2019), and economics (Apedaille et al., 1994; Edwards et al., 2020). The dynamics of predator-prey populations exhibit multiple wavelengths, beyond the generational oscillations predicted by Lotka-Volterra models. For example, the well-known Canada lynx–snowshoe hare system oscillates on a decadal timescale, which may be linked to climatic processes operating on centennial to millennial scales (Hone et al., 2011; Yan et al., 2013). Similar multiple-timescale oscillations have been observed in other systems and predicted theoretically (Laan and Hogeweg, 1995). These oscillations may reflect multi-generational evolutionary processes.

Long-term predator-prey dynamics are difficult to study due to the scarcity of population data on timescales beyond a century. The longest record known to us is the hare-lynx records of the Hudson Bay Company, which reflect a century of fur trade (Elton and Nicholson, 1942). Other records are much shorter, typically covering decades (Gilg et al., 2009; e.g., Vucetich et al., 2011). We propose that regional sets of radiocarbon-dated animal remains can be used to study predator-prey dynamics in deep time. Because radiocarbon can date materials up to 50,000 years old, it can extend the timescale for studying these important ecological interactions by three orders of magnitude.

Radiocarbon dating is best known for providing absolute dates for archaeological and paleontological organic materials, anchoring stratigraphic sequences and establishing the temporal context of specific findings. Large radiocarbon databases are also used in archaeology to infer changes in human demography (e.g., Stewart et al., 2021) or mammalian community structure (Lazagabaster et al., 2022). These demographic inferences are based on the "dates as data" paradigm, which assumes that the number of radiocarbon dates in a region reflects the magnitude of occupation or the total number of person-years of human existence (Rick, 1987). In paleontology, the probability of a specimen surviving to be dated is assumed to be proportional to the number of individuals of its taxon that existed in a specific region and time (Lazagabaster et al., 2022; Stuart and Lister, 2014). For example, radiocarbon data have been used to study megafaunal extinctions (Broughton and Weitzel, 2018; e.g., Stewart et al., 2021), using archaeological and paleoenvironmental data to assess the relative importance of anthropogenic and paleoclimatic drivers. Here, we address the more general question of whether the density of radiocarbon dates obtained from a regional set of paleozoological survey data can reveal long-term predator-prey population dynamics.

Radiocarbon data are inherently sparse, prone to selection and preservation biases, and subject to uncertainties arising from measurement error and calibration procedures used to adjust observed isotopic ratios to ancient background levels (Carleton, 2021; Hajdas et al., 2021; Reimer et al., 2020). Therefore, any attempt to infer ecological processes from radiocarbon dates should exercise caution, employing minimalist hypotheses, spatially constrained samples, and randomly collected specimens to minimize biases. Radiocarbon datasets spanning a wide time range with continuous deposition and multiple species occurrences are relatively resilient to sample size and effect size issues, and the number of dates in each SPD becomes less critical when identifying significant long-term trends (Crema, 2022; Hinz, 2020).

We found two datasets that meet the above criteria. The first is from eastern Beringia, where Fox-Dobbs et al. (2008) published radiocarbon dates of Late Pleistocene mammalian megafauna recovered from gravels near Fairbanks, Alaska. The Fairbanks data includes 33 wolves (*Canis lupus*), 28 horses (*Equus* sp.), and 3 reindeer (*Rangifer tarandus*), representing regional mortality between ~40-12 kya. The second dataset is from the Holocene (~10-0.5 kya) southern Judean Desert, Israel, where Lazagabaster et al. (2022) collected radiocarbon dates of leopard (*Panthera pardus nimer*, N = 12), hyrax (*Procavia*

capensis, N = 27), and Nubian ibex (*Cara ibex nubiana*, N = 10) from biogenic cave deposits. The Judean Desert data are argued to represent a random sample of the regional fauna (Lazagabaster et al., 2022).

We hypothesize that the summed probability distribution (SPD) of predator radiocarbon dates will differ from those of prey, with either greater or lesser divergence than expected from a random sample of SPDs from the same time range. This minimalist hypothesis assumes nothing about the wavelength, mechanism, or cause of predator-prey interaction, which we believe cannot be tested with the current data. If supported, this hypothesis would provide preliminary evidence that long-term regional radiocarbon data encode predator-prey interaction signals. This could justify constructing larger datasets to enable in-depth investigation of the structure of these signals.

Methods

The radiocarbon datasets, as detailed in Supplementary tables 1 and 2, were categorized into two groups for each region: predators (*Canis* / *Panthera*) and prey (*Equus*, *Rangifer* / *Procavia*, *Capra*). The original publications by Fox-Dobbs et al. (2008) and Lazagabaster et al. (2022) provide comprehensive information on the context and laboratory procedures, which are not reiterated here. The grouped radiocarbon ages underwent calibration (using the `rcarbon::calibrate` function) and were subsequently converted to Summed Probability Distributions (SPDs) using the `rcarbon::spd` function. These operations were performed in R 4.3.0 (R Core Team, 2021), utilizing the 'rcarbon' library developed by Crema and Bevan (2021).

Kullback-Leibler (KL) divergence, a widely used measure in information theory and data science, quantifies the difference between two probability distributions over a shared variable. Unlike symmetric measures, KL divergence is asymmetric, meaning the divergence of $p(x)$ from $q(x)$ differs from the divergence of $q(x)$ from $p(x)$. We chose KL divergence to compare SPDs due to its independence from arbitrary or predefined values and its reduced sensitivity to sample size, a common drawback of significance tests based on p-values (Crema, 2022).

KL divergence from the prey to the predator SPD was computed in each case using the `philentropy::KL` function from the 'philentropy' library (Drost, 2018). Following this, a random set of integers, equivalent to the sample size of the predator, was drawn from the range of the radiocarbon years of the prey. Each integer in the random set was assigned a radiocarbon measurement error that closely matched the real radiocarbon error in the actual dataset. These integers were then calibrated, converted to an SPD, and the Kullback-Leibler divergence from the actual prey SPD was calculated.

This random sampling procedure was repeated 100 times with replacement. The percentage of random samples was then used to estimate the likelihood of the divergence of the predator from the prey SPDs being derived from a random dataset, giving the probability of $KL(Predator||Prey) \notin KL(Random||Prey)$. The smoothed SPDs (calculated using 'modelbased::smoothing') are presented in the figures below. The smoothing procedure was applied subsequent to the KL divergence calculations.

Results and concluding remarks

The Fairbanks dataset shows fluctuating and alternating values of predator and prey densities over the interval between ~45 and 7 kya (Figure 1). The Kullback-Leibler (KL) divergence between the predator and prey distributions is 1.7174, which is smaller than 98% of the divergences measured for (random) predator-(real) prey distributions. This supports

our hypothesis that the Fairbanks predator and prey distributions are not random, and that the low divergence between them is therefore unlikely to be due to chance.

Similarly, the Judean Desert dataset shows fluctuating and alternating values of predator and prey densities over the interval between 10,000 and <500 years (Figure 2). The Kullback-Leibler (KL) divergence between the predator and prey distributions is 5.0741, which is smaller than 94% of the divergences measured for (random) predator-(real) prey distributions. This supports our hypothesis that the Judean Desert predator and prey distributions are not random, and that the low divergence between them is therefore unlikely to be due to chance.

Statistic		Fairbanks	Judean Desert
KL(Predator||Prey)		1.7174	5.0741
KL(Random||Prey)	Min.	1.559	3.065
	1st quartile	2.148	4.001
	Median	2.315	4.523
	Mean	2.294	4.417
	3rd quartile	2.473	4.858
	Max.	3.072	5.242
Bootstrap support for KL(Predator||Prey) ∉ KL(Random||Prey)		98%	94%

Table 1. Summary statistics of the original KL divergence of predator from prey SPD in the Fairbanks and the Judean Desert datasets.

As a specific case of population dynamics, predator-prey systems are typically studied over short time periods, limiting our understanding of long-term fluctuations driven by factors such as climate change and evolution. Radiocarbon records may capture signals of these dynamics under rare sampling conditions. Here, we tested the hypothesis that the divergence between predator and prey probability density curves is not random (KL(Predator||Prey) ∉ KL(Random||Prey)) using two coupled datasets from Fairbanks, Alaska, and the southern Judean Desert, Israel. Our results suggest that in these cases the divergence is unlikely to be random. This is informative of the idea that radiocarbon data may sequester long-term predator-prey interactions that are over and beyond the timescale observed until now. Additional high-resolution datasets are required to validate these results and further investigate the observed patterns.

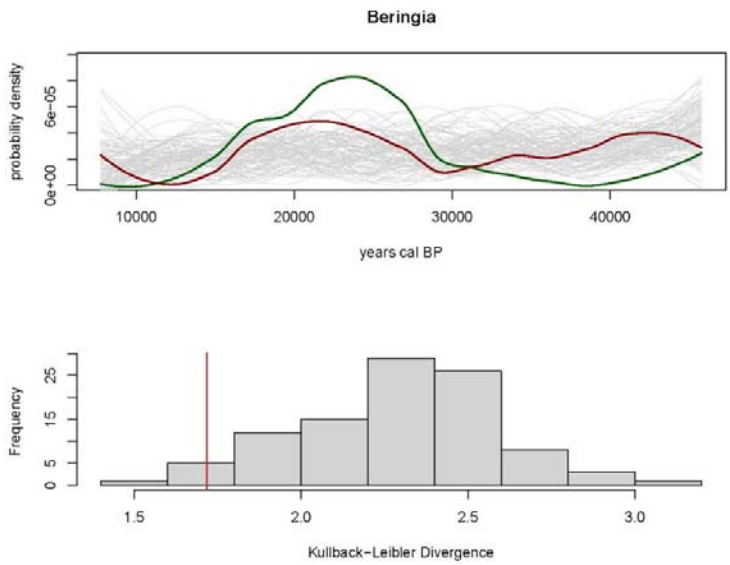

Figure 1. The prey (green) and predator (red) SPD for the Fairbanks data, against the background of 100 random SPD replicates. The distribution of the Kullback-Leibler divergences from the prey to the predator KL(Predator||Prey) SPDs is marked by the vertical red line on the histogram below, which shows the distribution of the KL divergences between the prey SPD and the random replicates KL(Random||Prey).[1]

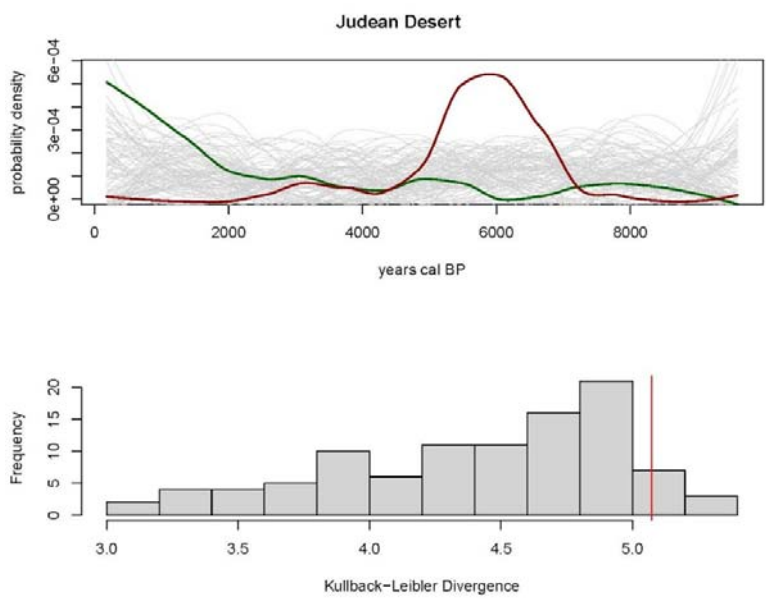

Figure 2. The prey (green) and predator (red) SPD for the Judean Desert data, against the background of 100 random SPD replicates.[2]

[1] The function was run with the following parameters: kld_dates(fairbanks_prey$RC_date, fairbanks_prey$RC_error, fairbanks_predator$RC_date, fairbanks_predator$RC_error, sample = 100, dataset_name = "Fairbanks", y_scaling_parameter = 4, smoothing = 0.4)

[2] The function was called with the following parameters: kld_dates(desco_prey$RC_date, desco_prey$RC_error, desco_predator$RC_date, desco_predator$RC_error, sample = 100, dataset_name = "Judean Desert", y_scaling_parameter = 4, smoothing = 0.4).

Appendices

Supplementary table 1. The Beringia dataset, from Fox-Dobbs et al. (2008, tables 2-3)

Genus	Specimen_ID	RC_date	RC_error	Lab_ID
Canis	AMNH F:AM 30450	7751	64	AA48695
Canis	AMNH F:AM 67165	12600	150	AA42317
Canis	AMNH F:AM 67157	14690	190	AA42315
Canis	AMNH F:AM 70944	15268	169	AA38449
Canis	AMNH F:AM 30447	15580	190	AA35223
Canis	AMNH F:AM 30451	15800	90	UCR3761
Canis	AMNH F:AM 67227	15870	190	AA35231
Canis	AMNH F:AM 68009-A	16800	210	AA35227
Canis	AMNH F:AM 67224	17640	240	AA35226
Canis	AMNH F:AM 30432	17670	230	AA48704
Canis	AMNH F:AM 30453	19210	260	AA48702
Canis	AMNH F:AM 70942	20150	110	CAMS115775
Canis	AMNH F:AM 67169	20305	385	AA35216A
Canis	AMNH F:AM 30452	20550	120	CAMS115769
Canis	CMN 9929	20910	70	UCR3764
Canis	AMNH F:AM 67231	21900	140	CAMS115774
Canis	AMNH F:AM 68008-G	23380	470	AA35222
Canis	AMNH F:AM 67170	27620	580	AA48694
Canis	AMNH F:AM 30431	28500	300	CAMS115776
Canis	AMNH F:AM 67248	29800	400	CAMS115773
Canis	AMNH F:AM 67168	31200	450	CAMS115767

Canis	CMN 42388	33900	1700	CAMS115763
Canis	AMNH F:A 67184	34600	700	CAMS115763
Canis	AMNH F:AM 67159	35200	2300	AA48703
Canis	AMNH F:AM 70958	37700	2600	AA37615
Canis	AMNH F:AM 70945	37733	2633	AA38448
Canis	AMNH F:AM 67202	38000	2700	AA35224
Canis	AMNH F:AM 67243	38500	1100	CAMS115772
Canis	CMN 17311	38790	540	UCR3762
Canis	AMNH F:AM 67197	39300	1230	CAMS115760
Canis	AMNH F:AM 67208	41040	1530	CAMS115759
Canis	AMNH F:AM 30438	45500	2700	CAMS115778
Canis	AMNH F:AM 67167	45800	2800	CAMS115768
Equus	AMNH F:AM 142429	12310	45	CAMS119982
Equus	AMNH F:AM 142423	12560	50	CAMS119976
Equus	AMNH F:AM 60025	13710	60	CAMS120061
Equus	AMNH F:AM 60005	14630	60	CAMS119969
Equus	AMNH F:AM 142421	14860	60	CAMS119974
Equus	AMNH F:AM 142424	15460	70	CAMS119977
Equus	AMNH F:AM 60032	15850	70	CAMS120068
Equus	AMNH F:AM 60004	16370	80	CAMS119968
Equus	AMNH F:AM 60044	18630	100	CAMS119970
Equus	AMNH F:AM 60023	19000	100	CAMS120058
Equus	AMNH F:AM 60027	19590	110	CAMS120059
Equus	AMNH F:AM 142420	19870	110	CAMS119973
Equus	AMNH F:AM 142430	19950	110	CAMS119983

Equus	AMNH F:AM 60020	19950	120	CAMS120062
Equus	AMNH F:AM 142427	19960	110	CAMS119980
Equus	AMNH F:AM 142426	20300	120	CAMS119979
Equus	AMNH F:AM 142425	20440	120	CAMS119978
Equus	AMNH F:AM 142419	20520	120	CAMS119971
Equus	AMNH F:AM 142428	21280	130	CAMS119981
Equus	AMNH F:AM 60026	21310	140	CAMS120060
Equus	AMNH F:AM 142435	21840	140	CAMS119989
Equus	AMNH F:AM 142434	22610	150	CAMS119988
Equus	AMNH F:AM 60003	24260	200	CAMS120077
Equus	AMNH F:AM 142431	25710	230	CAMS119985
Equus	AMNH F:AM 142433	25960	240	CAMS119987
Equus	AMNH F:AM 60033	39910	1330	CAMS120069
Equus	AMNH F:AM 60017	41000	1500	CAMS119972
Equus	AMNH F:AM 60221	43700	200	CAMS120067
Rangifer	AMNH F:AM 142443	16000	190	AA48686
Rangifer	AMNH F:AM 142444	16400	202	AA48687
Rangifer	AMNH F:AM 142440	16700	207	AA48682
Rangifer	AMNH F:AM 142441	17300	222	AA48683
Rangifer	AMNH F:AM 142438	21000	361	AA48680
Rangifer	AMNH F:AM 142446	29640	370	CAMS120070

Supplementary table 2. The Judean Desert Holocene dataset, modified from Lazagabaster et al. (2022).

Genus	Specimen_ID	Material	RCdate	RCerror	Laboratory	Lab_ID
Panthera	HE-004	collagen	5317	25	OxA	39091
Panthera	HE-008	collagen	5301	25	OxA	39214
Panthera	HE-010	collagen	4477	26	OxA	38732
Panthera	HE-053	collagen	4508	30	OxA	38788
Panthera	HE-054	collagen	6239	26	OxA	39216
Panthera	HE-124	collagen	5375	28	OxA	47465
Panthera	HE-195	collagen	4945	25	OxA	39107
Panthera	HE-230	collagen	4935	26	OxA	39109
Panthera	HE-231	collagen	5312	25	OxA	39110
Panthera	HE-232	collagen	5366	30	OxA	47473
Panthera	SK-703	bioapatite	3200	30	UGAMS	44190
Panthera	UR-035	bioapatite	8960	30	UGAMS	48266
Procavia	ARN-001	collagen	180	20	UGAMS	48283
Procavia	ARN-002	bioapatite	9600	110	UGAMS	48284
Procavia	C513-003	collagen	430	20	UGAMS	48261
Procavia	C513-004	collagen	1490	20	UGAMS	48260
Capra	EG-002	bioapatite	7850	30	UGAMS	46061
Procavia	EG-009	collagen	7141	28	OxA	-88
Procavia	HE-005	collagen	2948	22	OxA	39213
Capra	HE-021	collagen	3141	22	OxA	39215
Capra	HE-024	collagen	1860	20	UGAMS	46066
Procavia	HE-100	collagen	2920	20	UGAMS	46068
Procavia	HE-153	collagen	6476	26	OxA	39218
Procavia	HE-177	bioapatite	4350	20	UGAMS	46069
Procavia	HE-184	collagen	2920	22	OxA	39106
Procavia	HYS-002	collagen	1130	20	UGAMS	49003
Procavia	HYS-003	collagen	1280	20	UGAMS	49004
Procavia	QN-026	collagen	924	19	OxA	39255
Capra	QN-028	collagen	1870	20	OxA	39255
Procavia	QN-038	collagen	2520	30	UGAMS	46077
Procavia	QN-056	collagen	1144	20	OxA	39260

Capra	QN-083	collagen	4550	24	OxA	39175
Capra	QN-084	collagen	4520	20	UGAMS	46078
Procavia	QN-087	collagen	335	20	OxA	39176
Procavia	SK-001	collagen	363	22	OxA	39607
Procavia	SK-002	collagen	376	19	OxA	39608
Capra	SK-014	collagen	350	20	UGAMS	46081
Procavia	SK-046	collagen	1590	20	OxA	39609
Procavia	SK-152	bioapatite	6490	30	UGAMS	46134
Procavia	SK-189	collagen	1140	20	UGAMS	46085
Procavia	SK-211	collagen	4228	24	OxA	39930
Procavia	SK-241	collagen	620	18	OxA	39615
Procavia	SK-493	collagen	646	18	OxA	39849
Capra	TS-022	collagen	1338	20	OxA	39227
Capra	TS-032	collagen	1060	20	UGAMS	46116
Procavia	TS-065	collagen	1160	19	OxA	47371
Capra	TZB-004	collagen	870	20	UGAMS	48253
Procavia	TZB-009	collagen	2010	20	UGAMS	48251
Procavia	YO-013	collagen	721	18	OxA	39851

Acknowledgements

We thank Shimon Marom for his comments on the manuscript.

Data, scripts, code, and supplementary information availability

Data and code are available online: `https://zenodo.org/doi/10.5281/zenodo.10115388`

Conflict of interest disclosure

The authors declare that they comply with the PCI rule of having no financial conflicts of interest in relation to the content of the article.

Funding

We acknowledge the support of the DEADSEA_ECO ERC-Stg grant (#802752) awarded to NM.

References

Apedaille, L.P., Freedman, H.I., Schilizzi, S.G.M., Solomonovich, M., 1994. Equilibria and dynamics in an economic predator-prey model of agriculture. Math. Comput. Model. 19, 1–15.

Broughton, J.M., Weitzel, E.M., 2018. Population reconstructions for humans and megafauna suggest mixed causes for North American Pleistocene extinctions. Nat. Commun. 9, 5441.

Carleton, W.C., 2021. Evaluating Bayesian Radiocarbon□dated Event Count (REC) models for the study of long□term human and environmental processes. J. Quat. Sci. 36, 110–123.

Crema, E.R., 2022. Statistical Inference of Prehistoric Demography from Frequency Distributions of Radiocarbon Dates: A Review and a Guide for the Perplexed. Journal of Archaeological Method and Theory 29, 1387–1418.

Crema, E.R., Bevan, A., 2021. Inference from large sets of radiocarbon dates: software and methods. Radiocarbon.

Drost, H.G., 2018. Philentropy: Information Theory and Distance Quantification with R. Journal of Open Source Software.

Edwards, E.C., Go, D.-H., Oladi, R., 2020. Predator–prey dynamics in general equilibrium and the role of trade. Res. Energy Econ. 61, 101174.

Elton, C., Nicholson, M., 1942. The Ten-Year Cycle in Numbers of the Lynx in Canada. J. Anim. Ecol. 11, 215–244.

Fox-Dobbs, K., Leonard, J.A., Koch, P.L., 2008. Pleistocene megafauna from eastern Beringia: Paleoecological and paleoenvironmental interpretations of stable carbon and nitrogen isotope and radiocarbon records. Palaeogeogr. Palaeoclimatol. Palaeoecol. 261, 30–46.

Gilg, O., Sittler, B., Hanski, I., 2009. Climate change and cyclic predatorâ□□prey population dynamics in the high Arctic. Glob. Chang. Biol. 15, 2634–2652.

Hajdas, I., Ascough, P., Garnett, M.H., Fallon, S.J., Pearson, C.L., Quarta, G., Spalding, K.L., Yamaguchi, H., Yoneda, M., 2021. Radiocarbon dating. Nature Reviews Methods Primers 1, 1–26.

Hinz, M., 2020. Sensitivity of radiocarbon sum calibration. Journal of Computer Applications in Archaeology 3, 15.

Hone, J., Krebs, C.J., O'Donoghue, M., 2011. Is the relationship between predator and prey abundances related to climate for lynx and snowshoe hares? Wildl. Res. 38, 419–425.

Johnson, C.J., Mumma, M.A., St-Laurent, M.-H., 2019. Modeling multispecies predator–prey dynamics: predicting the outcomes of conservation actions for woodland caribou. Ecosphere 10, e02622.

Laan, J.D.V.D., Hogeweg, P., 1995. Predator—prey coevolution: interactions across different timescales. Proc. Biol. Sci. 259, 35–42.

Lazagabaster, I.A., Égüez, N., Ullman, M., Porat, R., Wachtel, I., Davidovich, U., Marom, N., 2022. Cave paleozoology in the Judean Desert: assembling records of Holocene wild mammal communities. J. Quat. Sci. 37, 651–663.

May, R.M., 2001 [1974]. Stability and Complexity in Model Ecosystems. Princeton University Press, Princeton & Oxford.

R Core Team, 2021. R: A Language and Environment for Statistical Computing.

Reimer, P.J., Austin, W.E.N., Bard, E., Bayliss, A., Blackwell, P.G., Ramsey, C.B., Butzin, M., Cheng, H., Lawrence Edwards, R., Friedrich, M., Grootes, P.M., Guilderson, T.P., Hajdas, I., Heaton, T.J., Hogg, A.G., Hughen, K.A., Kromer, B., Manning, S.W., Muscheler, R., Palmer, J.G., Pearson, C., van der Plicht, J., Reimer, R.W., Richards, D.A., Marian Scott, E., Southon, J.R., Turney, C.S.M., Wacker, L., Adolphi, F., Büntgen, U., Capano, M., Fahrni, S.M., Fogtmann-Schulz, A., Friedrich, R., Köhler, P., Kudsk, S., Miyake, F., Olsen, J., Reinig, F., Sakamoto, M., Sookdeo, A., Talamo, S., 2020. The IntCal20 Northern Hemisphere Radiocarbon Age Calibration Curve (0–55 cal kBP). Radiocarbon 62, 725–757.

Rick, J.W., 1987. Dates as Data: An Examination of the Peruvian Preceramic Radiocarbon Record. Am. Antiq. 52, 55–73.

Southall, B.L., Benoit-Bird, K.J., Moline, M.A., Moretti, D., 2019. Quantifying deep□sea predator–prey dynamics: Implications of biological heterogeneity for beaked whale conservation. J. Appl. Ecol. 56, 1040–1049.
Stewart, M., Carleton, W.C., Groucutt, H.S., 2021. Climate change, not human population growth, correlates with Late Quaternary megafauna declines in North America. Nat. Commun. 12, 965.
Stuart, A.J., Lister, A.M., 2014. New radiocarbon evidence on the extirpation of the spotted hyaena (Crocuta crocuta (Erxl.)) in northern Eurasia. Quat. Sci. Rev. 96, 108–116.
Vucetich, J.A., Hebblewhite, M., Smith, D.W., Peterson, R.O., 2011. Predicting prey population dynamics from kill rate, predation rate and predator-prey ratios in three wolf-ungulate systems. J. Anim. Ecol. 80, 1236–1245.
Yan, C., Stenseth, N.C., Krebs, C.J., Zhang, Z., 2013. Linking climate change to population cycles of hares and lynx. Glob. Chang. Biol. 19, 3263–3271.